Denoising for amplified Magnetic Resonance Imaging (aMRI)

Itamar Terem
iterem@stanford.edu

1. Abstract

Amplified MRI (aMRI) has been introduced recently as a new brain motion detection and visualization method, which enables one to dramatically amplify the brain tissue response due to blood pulsation and Cerebrospinal Fluid (CSF) motion. One limitation of aMRI is its sensitivity to noise. In this work, we evaluated the performances of different denoising algorithms, namely Non-Local Means (NLM), Block-Match and 3D Filtering (BM3D), and DnCNN for their ability to improve aMRI output in the present of different noise levels. Our analysis shows that even dough BM3D offered the highest PSNR and SSIM scores, there were no significant differences among the three algorithms, and that aMRI itself act as a strong denoiser.

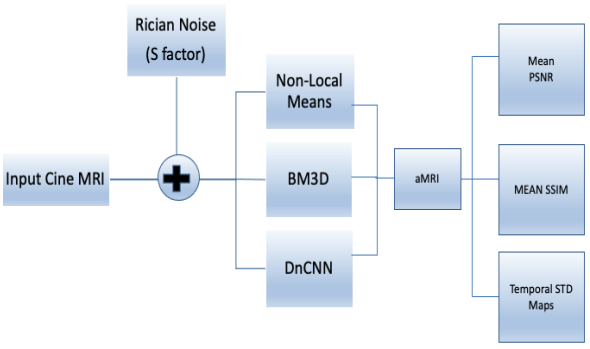

Figure 1. Flow diagram of the proposed project

2. Introduction

The physiological and biomechanical response of the human brain in vivo is thought to be altered in various neurological disorders [1, 2]. Thus, the ability to observe the manifestation of these disorders in the form of altered brain motion is thought to be of great interest.

Recently, amplified Magnetic Resonance Imaging (aMRI) has been introduced as a new brain motion detection and visualization method [3, 4, 5] which enables one to dramatically amplify the brain tissue response due to blood pulsation and Cerebrospinal Fluid (CSF) motion. aMRI takes as an input a 'cine' MR data and uses phase based motion magnification algorithms [6] to reveal the sub voxel motion of brain tissue. The algorithm performances are depended on the assumptions that the motion is sub-voxel and that the noise in the data is relatively low. Therefore, in the present of noise, motion artifacts can occur, which ultimately can lead to inaccurate diagnoses in patients. As a result, reducing the noise level in the data before applying the amplification algorithm is of great importance.

Several algorithms have been proposed for MRI denoising. For example, MRI denoising using Non-Local Means [7], which denoise the image by taking the mean of all pixels in the image, weighted by how similar these pixels are to the target pixel. In addition, Block Matching and 3D Filtering (BM3D) [8], which is enhanced technique of Non-Local Means filtering. Where instead of taking the mean of similar patches, a discrete wavelet transformation is applied, which result in sparse representation [9, 10]. The Denoising is achieved by shrinking (removing high frequency noises) the sparse spectrum, and inverse back to the image domain. Recently learning based approaches have been introduces. One of them is multi-channel residual learning of convolutional neural network (MCDnCNN) [11], which uses the basic DnCNN [12] algorithm, with multi-channel to denoise three dimensional MR images. Most of the denoising techniques in MRI were developed for a static MRI images, and do not take advantage of the spatio-temporal correlation among different frames. A recent conference paper by [13] was testing the combination of temporal and spatial denoising methods for cine MRI. In thier work, the temporal denoising was based on signal processing using the features of the noise, and the spatial denoising was performed for each frame by unsupervised network.

In this work, we evaluated the effects of different denoising algorithms, namely Non-Local Means, Block-Match and 3D Filtering (BM3D), and DnCNN for their ability to improve aMRI output in the present of different levels of noise.

3. Background/Related Work

Visualization of pulsatile brain motion with striking details was only recently achieved by amplified Magnetic Resonance Imaging (aMRI) [3, 4, 5]. several methods have been introduced in the past, among them Phase-contrast MRI, which enables direct measurements of the velocity blood and CSF flow [14], and a more recent quantitative tissue motion imaging technique, Displacement Encoded imaging with stimulated echoes (DENSE) MRI, which encodes tissue displacement in the phase of the stimulated echo [15]. aMRI can be viewed as a complementary method to both, because it enable the visualization of both CSF and brain tissue motion with great contrast, but does not enable direct quantification of the motion field.

As mentioned in the introduction section, most of the MRI denoising techniques [7, 8, 11] were developed for a static MRI data. A recent paper, by Peng [16] used Non-Local Mean to denoise 'cine' MRI data slice by slice, which is similar to the approach we adopted in this work. Another work by by Tsubasa [13] took this approach one step further and combined temporal and spatial denoising methods, in order to take advantage of the spatio-temporal correlation among the frames in the 'cine' MRI data.

In this work, we adopted the first approach used by [16], where each frame is independently denoised. A far as we know, this is the first time different denoising algorithms are tested for their ability to improve aMRI performances.

4. Method

4.1. Motion Magnification

aMRI is based on the Eulerian perspective for the flow field, where the properties of a voxel of fluid, such as pressure and velocity, evolve over time. This differs from the Lagrangian perspective, where the trajectory of particles is tracked over time. In the Eulerian approach to motion magnification, the motion is not explicitly estimated, but rather magnified by amplifying temporal intensity changes at fixed voxel [4, 5], assuming that the motion is subtle (sub-voxel).

aMRI starts by decomposing the data into scales and orientations using the 2D steerable pyramid (Fig 2). The scales (levels) basis functions are band pass filters in the frequency domain. They are calculated in polar coordinates by multiplying a low pass filter L_{s-1} of the previous scale with a high pass filter H_s of the current scale. The low pass and high pass filters for each scale are given by the following equations:

$$H_s(r) \begin{cases} 1, & \frac{r}{s} \geq 1 \\ \left| cos\left(\frac{\pi}{2} log_2\left(\frac{r}{s}\right)\right)\right|, & 0.5 < \frac{r}{s} < 1 \\ 0, & 0 < \frac{r}{s} \leq 0.5 \end{cases} \quad (1)$$

$$L_s(r) = \begin{cases} 0, & \frac{r}{s} \geq 1 \\ \left| sin\left(\frac{\pi}{2} log_2\left(\frac{r}{s}\right)\right)\right|, & 0.5 < \frac{r}{s} < 1 \\ 1, & 0 < \frac{r}{s} \leq 0.5 \end{cases} \quad (2)$$

Where s is the scaling factor of the level, and the band pass filter for the level is given by,

$$B_s(r) = H_s(r) \times L_{s-1}(r) \quad (3)$$

The angular filters satisfy the following equation in the frequency domain:

$$B_j(k_x, k_y) = \frac{(\alpha_j k_x + \beta_j k_y)^2}{k_x^2 + k_y^2}, \quad (4)$$

$j = 0, 2, 1, 3$

Where $\alpha_j = cos(\theta_j),\ \beta_j = sin(\theta_j)\ , and\ \theta_j = j\pi/3$. The resulting filter in the frequency domain for each level and orientation is given by:

$$A_{s,j}(k_x, k_y) = B_s(r) \times B_j(k_x, k_y) \quad (5)$$

Where, $r = \sqrt{k_x^2 + k_y^2}$

And every scale and orientation in the decomposition is constructed as follow:

$$I_{s,j}(x, y) = F^{-1}\left\{ F\left\{ I(x, y)\right\} \times A_{s,j} \right\} \quad (6)$$

Where s and j are the scaling factor and orientation direction respectively, $F\left\{ I(x, y)\right\}$ is the Fourier transform of the image, and F^{-1} is the inverse Fourier transform. The steerable pyramid decomposition outputs a complex number (amplitude and phase) at each scale and orientation. The phases are temporarily band-passed in order to isolate the cardiac temporal frequency and to remove any DC component. In addition, in order to enable motion magnification with minimal noise artifacts, the band-passed phases are spatially filtered with an amplitude-weighted Gaussian

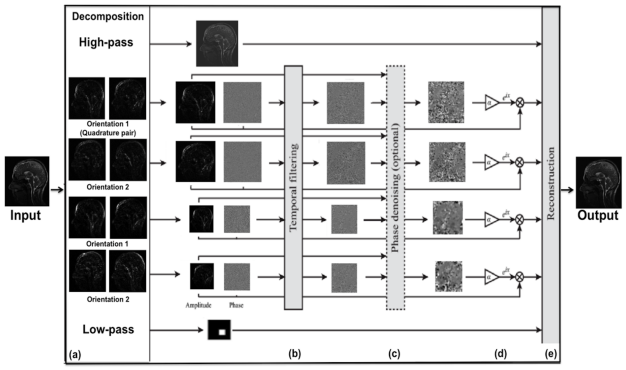

Figure 2. The amplification algorithm described by Wadhwa et al. [6], as applied to MRI cine data. (A) The cine MRI (short video) is decomposed by the complex steerable pyramid into scales and orientations. (B) The phases are independently temporally filtered at each spatial location, orientation, and scale. (C) The filtered phases are spatially filtered again to increase the phase SNR using amplitude-weighted Gaussian spatial smoothing. (D) The filtered phases are multiplied by an amplification parameter and added to the original phase components, and finally the video is reconstructed (E)

smoothing filter. Next, the band-passed phases are multiplied by a user-defined amplification factor, α, and added to the original phase component. Attenuation of motion of the other temporal frequencies is achieved by adding the band-passed phases to a reference phase image, which in our case was chosen to be the first image. The movie is then reconstructed to synthesize an amplified movie with the desirable range of temporal frequencies.

I this work, the same parameters as in the original paper [4] were used as a based line: amplification factor $\alpha = 15$, band-pass filter of the heart rate frequency (± 0.1) in addition to attenuating the motion related to all other temporal frequencies, and amplitude-weighted Gaussian smoothing with $\sigma = 5$. This parameters supports sufficient amplification and with minimum artifacts and distortions.

4.2. Denoising

4.2.1 Non-Local Means

The Non-Local Means (NLM) algorithm was first propose by Buades et al. [17], and is based on the fact that natural images have some self spatial similarity. In this approach the image is denoised by taking the mean of all pixels (or patches) in the image and weighted them by how similar they are relative to the target pixel. The weights are Gaussian function of the similarity between patches, and the its measured as the L2 norm of the patch and target pixels. This results in different weighting for different patches, where high similarity result in greater weight and vice versa.

4.2.2 Block Matching and 3D Filtering

The BM3D [9, 10] is an extentios of the Non-Local Means algorithm, where instead of taking the mean of all similar patches a 3D matrix is constructed, and decomposed by a 3D unitary sparsifying transform. The sparse representation is then threshold and Weiner filtered in order to achieve coefficient shrinkage to remove high frequency noises. The filtered block is then inverse transform which result in a denoise 3D block. The denoise target patch is then estimated by taking the weight-averaged of all patches is the block. In both Non-Local Means and BM3D the algorithm performance depends on the size of the searching window, and other hyper parameters.

4.2.3 DnCNN

DnCNN [12] is a denoising convolutional neural networks that estimate the noise (residual image) from the Gaussian noisy input image. The denoise image is estimated by taking the difference between the noisy image and the residual (noise) image. The algorithm utilized residual learning and batch normalization to improve the denoising performance and to speed up training. In addition, compared to other models, which usually train to denoise an image with specific additive white Gaussian noise level, DnCNN model is able to handle Gaussian denoising with unknown noise level (i.e., blind Gaussian denoising) [12].

5. Analysis & Evaluation

MR images are reconstructed from the sampled complex spatial frequency data, and as a result the image itself is complex in nature. The input to the aMRI algorithm are the magnitude images of the original complex images. When taking the magnitude of the complex images, the noise distribution is changing. In the complex representation, both the real and the imaginary parts contain additive zero-mean Gaussian noise, so the magnitude image noise distribution is no longer Gaussian, but rather Rician [18].

In this work, we used Non-Local Means, BM3D and DnCNN algorithms to denoise the MRI videos. Because the aMRI algorithm has denoising elements in it (amplification and amplitude weighted Gaussian smoothing) the NLM and BM3D were tested with default parameters (the search window size for similar patches was set to 21 pixels, and the comparison window size was set to 5 pixels). We chose this approach, because this preliminary work was mainly focus on testing the general effect of denoising algorithms on the aMRI performances, and not on optimizing their hyper parameters.

The amplify videos were evaluated qualitatively and quantitatively. Qualitative analysis was done by visually comparing the amplify denoised videos, and by generat-

ing normalize temporal standard deviation (STD) maps to enable the observation of motion artifacts and noise in the form of 2D images. Quantitative analysis was done by calculating the peak signal to noise ratio (PSNR) and the structural similarity Index (SSIM) between each of the frames in the amplified denoised video and the reference video (amplification without noise). The PSNR and SSIM scores were calculated over the brain tissue, excluding the background.

We started by adding Rician noise, with varying S parameter (ranging from 0 - 0.1) to the original video, resulting in a noisy video. The noisy video was then denoised using the three denoising algorithms (Non-Local Means, BM3D and DnCNN). For reference, we first computed the PSNR and the SSIM scores between the denoised video and the original video. We continued by amplifying the denoised videos using the aMRI algorithm, and analyzed the resulting videos using the metrics defined above (PSNR, SSIM and STD maps).

For the next analysis a single Recian $S = 0.025$ factor was tested. This factor was chosen empirically. We visually noticed that when using the default aMRI parameters as in the original paper, the motion in the amplified videos for $S > 0.02$ contain significant amount of motion artifacts. As a result, we wanted to test different amplification factors ([2.5 - 20]) and thier effect on the performances of the denoising algorithms for a fixed S parameter. The resulting videos were compared in the same fashion mentioned above.

Finally, we tested the effect of the amplitude Gaussian smoothing filter on the performances of the denoising algorithms for a fixed $S = 0.025$ parameter, by varying sigma ([2.5 - 15]). We then compared the the resulting videos in the same fashion mentioned above.

6. Results

6.1. Denoising Without Amplification (Reference)

We started by evaluating the performances of the denoising algorithms without applying any magnification. Table 1 shows the temporal mean PSNR and SSIM for Rician noise $S = 0.025$ parameter, and for each of the denoising methods. As can be seen, BM3D got significantly higher scores (PSNR 36.683 & SSIM 0.959) for both evaluation measurements, compared to NLM and DNCNN which got PSNR score of 33.705 and 34.157, and SSIM score of 0.921 and 0.920 respectively.

denoising Algorithm	Mean PSNR	Mean SSIM
Non-Local Means	33.705	0.921
BM3D	36.683	0.959
DnCNN	34.157	0.920

Table 1: Mean PSNR and SSIM for Rician noise factor of $S = 0.025$ for the three denoising algorithms without applying magnification

Figure 3 & 4 depict the PSNR and SSIM scores for each of the denoising methods as a function of the Rician noise S parameter. As can be seen, the BM3D algorithm performs the best over the varying S parameters, although for large level of noise ($S = 0.1$) DnCNN and BM3D the PSNR scores are almost the same.

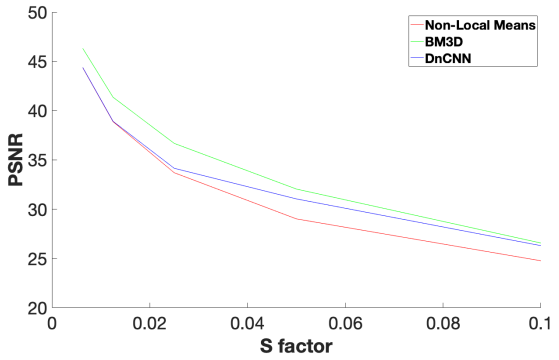

Figure 3. PSNR score as a function of Rician noise S factor for the three denoising algorithms without amplification

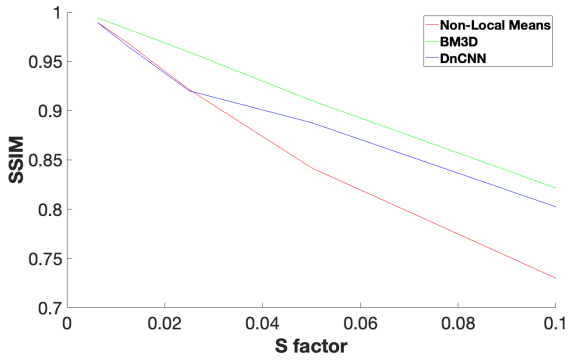

Figure 4. SSIM score as a function of Rician noise S factor for the three denoising algorithms without amplification

Figure 5 & 6 depict anatomical snapshot, and the normalize temporal standard deviation maps of the original cine MRI, and the denoised videos for Rician noise level $S = 0.025$. The largest PSNR score (36.683) was obtained by BM3D, although visually the DnCNN result looks better (subjectively). In addition, compared to the reference STD maps, large amount of variation was observed for all the three algorithms.

6.2. Denoising with Amplification

The next step was to evaluate the performances of the denoising algorithms after amplification. Table 2 shows the mean PSNR and SSIM for Rician noise $S = 0.025$ parameter, and for each of the denoising methods. As can be seen,

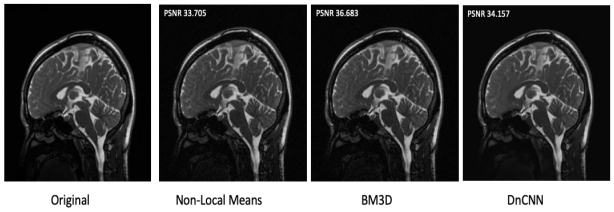

Figure 5. Anatomical snapshots of the denoised videos without amplification

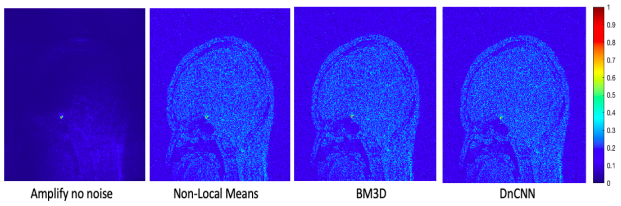

Figure 6. Normalize temporal standard deviation maps for Rician factor of $S = 0.025$ of the denoised videos without amplification

compared to the non-amplified results there is an improvement in the PSNR score for NLM and DnCNN, but reduced PSNR score for BM3D. Notice that the PSNR and SSIM scores for the three denoising algorithms are not significant different. Also notice, that the PSNR and SSIM scores for the reference video (noisy amplified video) are significantly smaller compared to the scores obtained after the denoising algorithms.

denoising Algorithm	Mean PNSR	Mean SSIM
Noisy Video (reference)	34.078	0.941
Non-Local Means	34.517	0.949
BM3D	34.599	0.950
DnCNN	34.374	0.948

Table 2: Mean PSNR and SSIM for Rician noise factor of $S = 0.025$ for the three denoising algorithms after magnification

Figure 7 & 8 depict the PSNR and SSIM scores for each of the denoising methods as a function of the Rician noise S parameter. As can be seen, for $S > 0.02$, the PSNR and SSIM scores for the noisey video are smaller compared to the denoising results. Surprisingly, for $S < 0.025$ the scores for the noisy and denoised videos is almost identical. Another surprise is the fact that the PSNR scores for the three denoising methods are almost the same for all S factors. The SSIM plot almost exhibit the same trend, although here the DnCNN and BM3D are a bit superior to Non-Local Means.

Figure 9 depicts the normalize temporal standard deviation maps of the amplify denoised videos for Rician noise level $S = 0.025$. The overall motion characteristic in the

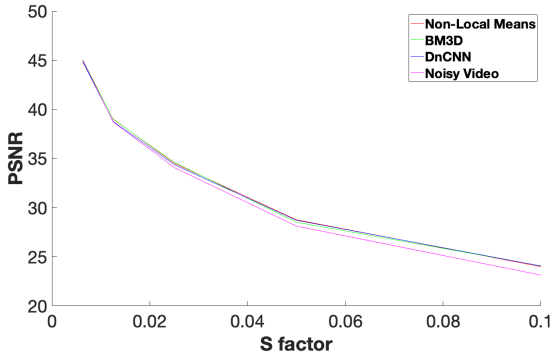

Figure 7. PSNR score as a function of Rician noise S factor for the three denoising algorithms with amplification

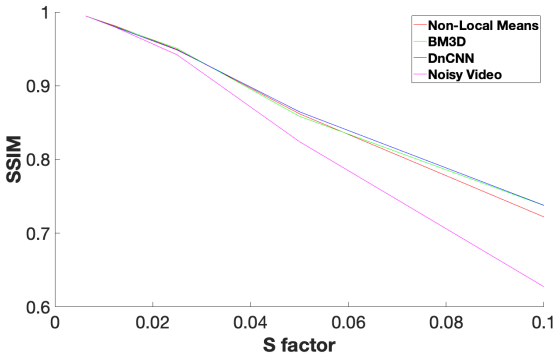

Figure 8. SSIM score as a function of Rician noise S factor for the three denoising algorithms with amplification

brainstem (midbrain, pons, and medulla) together with the lateral ventricles is comparable with the reference standard deviation map (amplification without noise addition) for all the three denoisisng methods. contrary, large noise level can be observed in the cortex area in all the three denoising STD maps. This noise appear in the magnified movies as mixture of noise and motion artifacts (all the results for all the experiments can be generated using the code and data in the GitHub repository).

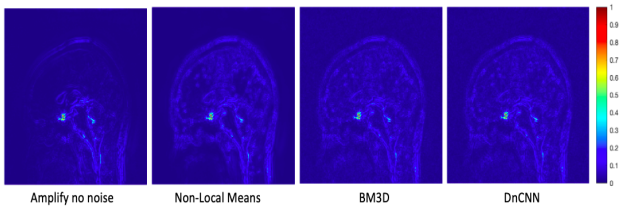

Figure 9. Normalize temporal standard deviation maps for $Rician$ factor of S = 0.025 of the denoised videos with amplification

6.3. Varying Amplification Factor

As mentioned in the motion magnification section, motion artifacts can occur when the magnification factor is too large, which in turn will affects the qualitative and quantitative scores. Therefore, the affect of different amplification factor on the PSNR and SSIM scores was tested. Figure 10 & 11 depict the PSNR and SSIM scores for each of the denoising methods as a function of amplification factor. As can be seen, for fix noise level (S = 0.025) the BM3D algorithm exhibit the best scores for both measurements, but with minimal difference among the three methods. In addition, the PSNR plot exhibit a peak at 7.5 amplification factor for all denoising algorithms (including the reference data). Another observation worth paying attention to is the fact that the SSIM score remain constant (more or less) up to amplification factor of 7.5, and then starts to decrease.

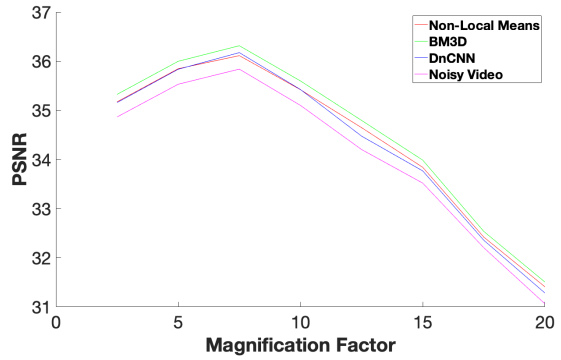

Figure 10. PSNR score as a function of amplification factor for the three denoising algorithms

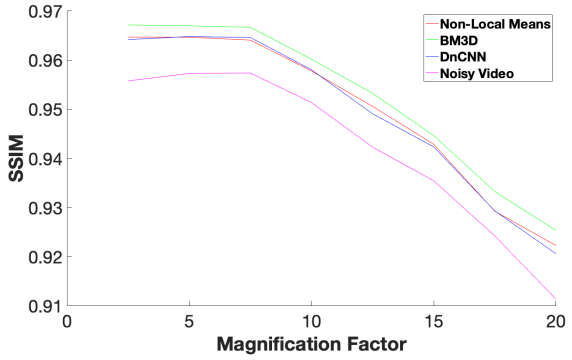

Figure 11. SSIM score as a function of amplification for the three denoising algorithms

Figure 12 depicts the normalize temporal standard deviation maps of the amplify denoised videos for Rician noise level $S = 0.025$, and for amplification factor of 7.5 (the magnification with the largest PSNR). As before, overall the motion characteristic in the brainstem (midbrain, pons, and medulla) together with the lateral ventricle for all the three denoisisng methods is comparable with the reference standard deviation map (amplification without noise addition). Even dough the cortex in all of the denoising STD contains a lot of noise, for this magnification factor, the noise does not appear as motion artifact in the magnified videos, but rather as a pure temporal noise.

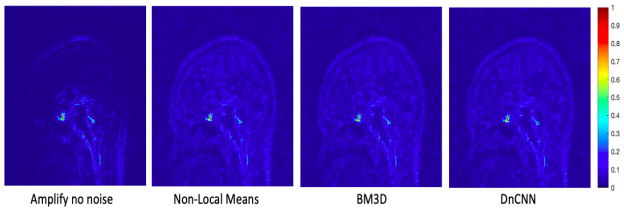

Figure 12. Normalize temporal standard deviation maps for amplification factor of 7.5 for the denoised videos

Table 3 shows the PSNR and SSIM scores for amplification factor of 7.5 for the three denoising methods. As can be seen, there is a significant improvement in the PSNR and SSIM scores for the three methods, compared to both the noisy amplified and not-amplified results with a fixed S factor of 0.025, but not significant difference among them.

denoising Algorithm	Mean PNSR	Mean SSIM
Noisy Video (reference)	35.838	0.957
Non-Local Means	36.113	0.964
BM3D	36.314	0.966
DnCNN	36.174	0.964

Table 3: PSNR and SSIM score for amplification factor of 7.5 for the three denoising algorithms

6.4. Varying Sigma Parameter

As we saw in the motion magnification section, one way to mitigate motion artifact in the resulting amplified videos is using an Amplitude-Weighted Gaussian Filter. In this part, we wanted examined the affect of the Gaussian variance on the PSNR and SSIM scores. Figure 13 & 14 depict the PSNR and SSIM scores for each of the denoising methods as a function of different sigma values, for a fixed noise level (S = 0.025). As can be seen, the BM3D algorithm exhibit the best scores for both measurements, but with not significant difference. In addition, notice that the scores grow with larger sigmas due to the affect of smoothing. This of course come on the expense of losing motion information (Fig 15).

Figure 15, depict the normalize temporal standard deviation maps for sigma of 7.5 for the denoised videos. We chose to display the result with sigma of 7.5, because we noticed that for sigma values greater than 7.5 we start to loose some of the motion information due to the large affect

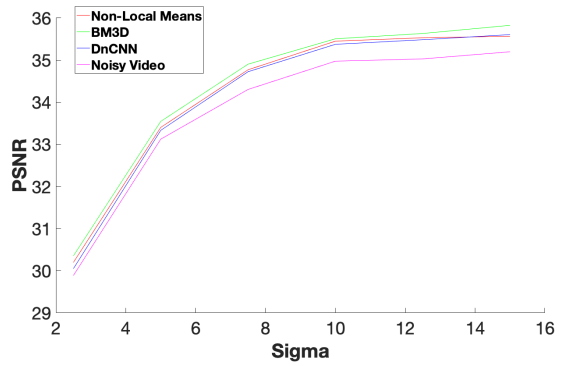

Figure 13. PSNR score as a function of sigma values for the three denoising algorithms

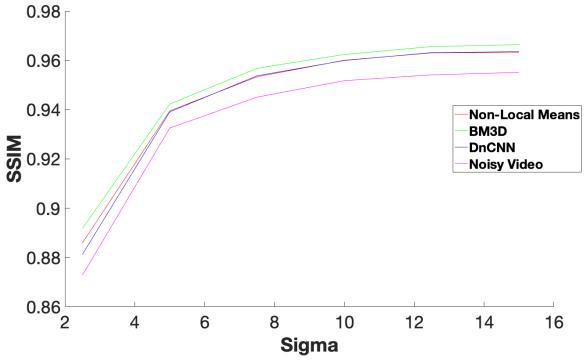

Figure 14. SSIM score as a function of sigma values for the three denoising algorithms

of smoothing. As can be seen, the motion in the brainstem (midbrain, pons, and medulla) together with the lateral ventricle is almost identical to the reference video for the three denoising methods. Even dough the cortex is still noisy, the output videos exhibit enough magnification with some small motion artifacts.

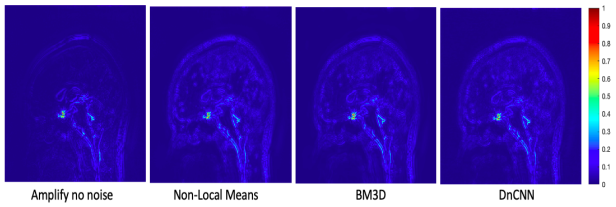

Figure 15. Normalize temporal standard deviation maps for sigma of 7.5 for the denoised videos

Table 3 shows the PSNR and SSIM scores from sigma value of 7.5 for the three denoising methods. As can be seen, there is a significant improvement in the PSNR and SSIM scores for the three methods, compared to the noisy amplified video with the same Rician noise S factor, but now significant difference was observed among the denoising methods.

denoising Algorithm	Mean PNSR	Mean SSIM
Noisy Video (reference)	34.304	0.945
Non-Local Means	34.771	0.953
BM3D	34.904	0.956
DnCNN	34.725	0.953

Table 4: PSNR and SSIM score for sigma of 7.5 for the three denoising algorithms

7. Discussion & Conclusion

This work was tested the effects of three well known denoising algorithms, Non-Local Means (NLM), Block-Match and 3D Filtering (BM3D), and DnCNN and their ability to improve the performances of amplified Magnetic Resonance Imaging (aMRI) in the present of different noise levels. The focus of this work was to test the general effects of denoising algorithms on aMRI performances. As a result the algorithms were tested with default parameters, and without hyper parameters optimization. Normalize temporal standard deviation maps, PSNR and SSIM scores were used to evaluate the performances of the denoising algorithms.

We started first by denoising the videos without applying magnification as a reference baseline. The results (Fig 3 & Fig 4) showed that BM3D was most successful in noise removal, especially for low level of noise ($S < 0.02$). The PSNR and SSIM scores (Table 1), show the superiority of BM3D over NLN and DnCNN. It is important to mentioned that the DnCNN algorithm was trained on natural images with Gaussian noise, but as mentioned in the Analysis and Evaluation section, the magnitude MR images are characterized by Rician noise. That could explain the low level performances of the DnCNN compared to BM3D. Another important observation is the residual remaining temporal noise (Fig 6) in the denoised videos. This residual noise is mainly due to the facts that each frame was denoised independently, and did not take into account the spatio-temporal correlation among the frames.

For our the second analysis, the denoised videos were amplified using aMRI with default parameters. Her, the results (Fig 7 & Fig 8) were a bit surprising. For noise level of $S < 0.02$ there were very little PSNR and SSIM scores difference among all denoising method including the reference video (magnification without denoising). These suggest that that the aMRI algorithm itself act as a denoiser. This can be explained by the following:

1. In the phase based motion magnification approach, while the amplification factor is increased, noise is translated rather than amplified, which result in larger SNR.

2. The amplitude weighted Gaussian smoothing filter, further increase the SNR.

3. Attenuating other temporal frequencies, further reduce the noise and increase the overall SNR.

For larger level of noise ($S > 0.02$) a difference in PSNR and SSIM score between the reference video and the denoising videos was observed, but surprisingly there was not significant difference among the denoising algorithm. This is especially surprising, because the first analysis (denoising without amplification) showed difference, which apparently did not propagated to the amplified outputs. This suggests that the overall denoising affects of aMRI are stronger than those of the denoising algorithms. The STD maps (Fig 9) showed that the motion in the mid-brain region in the amplified denoised outputs is comparable to the reference video, but contain a significant amount of noise in the cortex. High level of noise ($S > 0.02$) resulted in non realistic motion apparent in the amplified output. This can lead to misinterpretation in future disease diagnosis using aMRI.

In the third analysis, the denoised videos were amplified using different amplification factor. The results (Fig 10 & Fig 11), showed that the PSNR and SSIM score depends on the amplification factor. The PSNR was growing with the amplification factor, and exhibit a peak at $\alpha = 7.5$. This shows again the denoising affects aMRI has, and that they are stronger then the denoising algorithm affects. In addition, compared to the previous section, the PSNR score increased in all three algorithm by almost 2dB, but yet minimal differences was observed among them.

In our last analysis, the denoised videos were amplified using different sigma parameters in the amplitude based Gaussian smoothing. As expected increasing the sigma resulted in better PSNR and SSIM scores (Fig 13 & Fig 14), but also resulted in lower motion detection resolution. The STD maps (Fig 15) showed that sigma = 7.5 resulted in motion resolution similar to the reference video. As before, we noticed that the PSNR and SSIM scores (Table 4) for all denoising methods is better then the reference video, but almost the same among them (0.02 db differences between BM3D and NLM and DNCNN).

In this work we tested the effects of different denosing algorithm on aMRI performance. Our analysis suggests that there is a benefit for applying denoising algorithm before using aMRI (PSNR increased in around 0.5 dB compared to the reference noisy video). In addition, our analysis shows that even dough BM3D offered the highest PSNR and SSIM scores, there were no significant differences among the three algorithms, and that aMRI itself act as a strong denoiser. Future work will need to test this claim further, by first optimizing the algorithms hyper parameters, and by adopting spatio-temporal denoising algorithms, which take into account the correlation among the video frames. This is especially of great importance, because as observed the denoised videos contained a lot of residual temporal noise, which suggests that the denoise results can be improved further. In addition, testing different deep learning algorithms which was trained on brain MRI images with Rician noise (compared to DnCNN) will probably improve the results significantly.

References

[1] Bradley WG Jr. Magnetic resonance imaging of normal pressure hydrocephalus. *Semin Ultrasound CT MR*, 37(2):120–128, 2016.

[2] Tsao et al. Relations of arterial stiffness and endothelial function to brain aging in the community. *Neurology*, 81(2):984–991, 2013.

[3] Samantha J Holdsworth, Mahdi Salmani Rahimi, Wendy W Ni, Greg Zaharchuk, and Michael E Moseley. Amplified magnetic resonance imaging (aMRI). *Magn. Reson. Med.*, 75(6):2245–2254, 2016.

[4] Itamar Terem, Wendy W Ni, Maged Goubran, Mahdi Salmani Rahimi, Greg Zaharchuk, Kristen W Yeom, Michael E Moseley, Mehmet Kurt, and Samantha J Holdsworth. Revealing sub-voxel motions of brain tissue using phase-based amplified MRI (aMRI. *Magn. Reson. Med.*, 80(6):2549–2259, 2018.

[5] I Terem, L Dang, A Champagne, J Abderezaei, A Pionteck, Z Almadan, AM Lydon, M Kurt, M Scadeng, and SJ. Holdsworth. 3d amplified mri (amri). *Magn Reson Med.*, 86(3):1674–1686, 2021.

[6] Neal Wadhwa, Michael Rubinstein, Frédo Durand, and William T Freeman. Phase-based video motion processing, 2013.

[7] JV Manjón, J Carbonell-Caballero, JJ Lull, G García-Martí, Martí-Bonmatí, and Robles M L. Mri denoising using nonlocal means. *ed Image Anal*, 12(4):514–523, 2008.

[8] V Hanchate and K Joshi. Mri denoising using bm3d equipped with noise invalidation denoising technique and vst for improved contrast. *Med Image Anal.*, 234(2), 2020.

[9] K Dabov, A Foi, V Katkovnik, and K Egiazarian. Image denoising by sparse 3-d transform-domain collaborative filtering. *IEEE Trans Image Process*, 16(8):2080–2095, 2007.

[10] K Dabov, A Foi, V Katkovnik, and K Egiazarian. Bm3d image denoising with shape-adaptive principal component analysis. *Proceedings workshop on signal processing with adaptive sparse structured representations*.

[11] D Jiang, W Dou, L Vosters, X Xu, Y Sun, and T Tan. Denoising of 3d magnetic resonance images with multi-channel residual learning of convolutional neural network. *Jpn J Radiol*, 36(9):566–574, 2018.

[12] Zhang K, Zuo W, Chen Y, Meng D, and Zhang L. Beyond a gaussian denoiser: Residual learning of deep cnn for image denoising. *IEEE Trans. Image Process*, 26(7):3142–3155, 2018.

[13] Maeda Tsubasa, Tamura Satoshi, and Kawaji Satoru, Hayamizu ans Keigo. Combination of temporal and spatial denoising methods for cine mri. *2021 IEEE 3rd Global Conference on Life Sciences and Technologies (LifeTech 2021)*.

[14] Pelc N Enzmann DR. Brain motion measurement with phase-contrast mr imaging. *Radiology*, 185(9):653–660, 1992.

[15] Xiaodong Zhong et at. Balanced multipoint displacement encoding for dense mri. *Magn Reson Med*, 61(4):981–988, 2009.

[16] Y Peng, X Su, Let Hu, and al. Feasibility of three-dimensional balanced steady-state free precession cine magnetic resonance imaging combined with an image denoising technique to evaluate cardiac function in children with repaired tetralogy of fallot. *Korean J Radiol*, 22(9):1525–1536, 2021.

[17] Antoni Buades, Coll Bartomeu, and Morel. Jean-Michel. A non-local algorithm for image denoising. *Computer Vision and Pattern Recognition*, 2.

[18] Hkon Gudbjartsson and Patz. Samuel. The ri- cian distribution of noisy mri data. *Magnetic resonance in medicine*, 34(6):910–914, 1995.

8. Supplementary Materials

Please see the following link to view all code resources used in the development of our project: `https://github.com/ItamarTerem/EE-367-Project-Denoising-aMRI.git`